SIMULATION AND ANALYSIS OF A TISSUE EQUIVALENT PROPORTIONAL COUNTER USING THE MONTE CARLO TRANSPORT CODE FLUKA

A Thesis

by

JEREMY DELL NORTHUM

Submitted to the Office of Graduate Studies of
Texas A&M University
in partial fulfillment of the requirements for the degree of

MASTER OF SCIENCE

May 2010

Major Subject: Health Physics

SIMULATION AND ANALYSIS OF A TISSUE EQUIVALENT PROPORTIONAL COUNTER USING THE MONTE CARLO TRANSPORT CODE FLUKA

A Thesis

by

JEREMY DELL NORTHUM

Submitted to the Office of Graduate Studies of
Texas A&M University
in partial fulfillment of the requirements for the degree of

MASTER OF SCIENCE

Approved by:

Chair of Committee,	Stephen B. Guetersloh
Committee Members,	Leslie A. Braby
	Katherine M. Jackson
Head of Department,	Raymond J. Juzaitis

May 2010

Major Subject: Health Physics

ABSTRACT

Simulation and Analysis of a Tissue Equivalent Proportional Counter Using the Monte Carlo Transport Code FLUKA. (May 2010)

Jeremy Dell Northum, B.S., Texas A&M University

Chair of Advisory Committee: Dr. Stephen Guetersloh

The purpose of this study was to determine how well the Monte Carlo transport code FLUKA can simulate a tissue-equivalent proportional counter (TEPC) and produce the expected delta ray events when exposed to high energy heavy ions (HZE) like in the galactic cosmic ray (GCR) environment. Accurate transport codes are desirable because of the high cost of beam time, the inability to measure the mixed field GCR on the ground and the flexibility they offer in the engineering and design process.

A spherical TEPC simulating a 1 μm site size was constructed in FLUKA and its response was compared to experimental data for an ^{56}Fe beam at 360 MeV/nucleon. The response of several narrow beams at different impact parameters were used to explain the features of the response of the same detector exposed to a uniform field of radiation. Additionally, an investigation was made into the effect of the wall thickness on the response of the TEPC and the range of delta rays in the tissue-equivalent (TE) wall material. A full impact parameter test (from IP = 0 to IP = detector radius) was performed to show that FLUKA produces the expected wall effect. That is, energy

deposition in the gas volume can occur even when the primary beam does not pass through the gas volume.

A final comparison to experimental data was made for the simulated TEPC exposed to various broad beams in the energy range of 200 – 1000 MeV/nucleon. FLUKA overestimated energy deposition in the gas volume in all cases. The FLUKA results differed from the experimental data by an average of 25.2 % for y_F and 12.4 % for y_D. It is suggested that this difference can be reduced by adjusting the FLUKA default ionization potential and density correction factors.

ACKNOWLEDGEMENTS

I would like to thank my committee members: Dr. Stephen Guetersloh, Dr. Leslie Braby and Dr. Kathy Jackson for all of their help with this thesis. This would not have been possible without their help. I would also like to acknowledge the San Antonio Lighthouse for their support over the years. Lastly, I would like to thank my parents, James and Tonia, for always supporting me in my pursuit of an education.

TABLE OF CONTENTS

Page

LIST OF FIGURES

FIGURE Page

FIGURE Page

LIST OF TABLES

CHAPTER I

INTRODUCTION

The study is motivated by NASA's need to minimize uncertainties associated with radiation exposures for long-term deep space travel. A tissue-equivalent proportional counter (TEPC) has been used as a dosimeter in mixed radiation fields. Since it does not measure linear energy transfer (LET) directly, the response function must be characterized in order to estimate quality factor and thus dose equivalent for the incident radiation. The objectives of this study are to simulate the measured response of a spherical TEPC, similar to one flown on the ISS, exposed to high-energy heavy ions (HZE) in the galactic environment by simulation using Monte Carlo methods. Simulations of heavy ion interactions using the FLUKA Monte Carlo transport code will be compared with measurements of energy deposition in a spherical TEPC. Due to the wealth of data existing for ^{56}Fe at 360 MeV/nucleon (Gersey 2002), this beam was chosen as a reference.

Simulations of heavy ion interactions using the FLUKA Monte Carlo transport code will be compared with measurements of energy deposition in a spherical TEPC. The cell nucleus is a principal target for radiation injury because it contains virtually all of the DNA in the cell (Rossi 1996). Since its dimensions are on the order of micrometers, a 1 μm site size is appropriate for studying the energy deposition in a cell nucleus.

This thesis follows the style of Health Physics.

Since a site size of 1 μm was chosen for the sensitive volume of the detector in the experiment, energy escaping the volume by delta ray transport away from the point of interaction becomes an issue for Monte Carlo transport simulations. FLUKA has all of the components necessary for this study as it transports delta ray electrons and has the ability to track nuclear collisions resulting in fragmentation of the projectile and target atoms. Work prior to this study confirms that FLUKA can accurately simulate patterns of energy deposition in microscopic volumes as well as microdosimeters simulating those sizes. It is therefore a valuable tool not only for improving the design of the next generation of detectors, but also for understanding the operation of existing instruments without the need for costly flight time.

TEPCs have existed for close to 50 years and have been very well characterized (Rossi 1996). The distributions to be simulated have been measured as early as the 1960s. However, it is only recently (within the past 10 years) that such experiments have been simulated on a regular basis with Monte Carlo codes. Similar studies have been performed with MCNP (Hoff 2002) and GEANT4 (Wang 2006).

A literature search revealed FLUKA has been used to simulate TEPCs (Beck 2005; Fasso 2003; Rollet 2004). In these cases, however, FLUKA was used to model very specific detectors in very specific experimental arrangements. As stated earlier, the goal of this research is to study how well FLUKA can produce the expected delta ray events. That is, how well it can simulate the physical processes common to all TEPCs, not just how well it can simulate a very specific experiment. If simulation and transport methods prove accurate, much time can be saved in the design phase of new instruments

as expensive beam time characterization may be minimized. To achieve this goal, a consistent, generic TEPC design was chosen for each beam orientation along with a consistent beam (^{56}Fe at 360 MeV/nucleon). The TEPC will be analyzed on many levels including but not limited to: wall effects, response to beams of different orientations and with and without FLUKA transporting delta rays (referred to as delta rays "on" and delta rays "off," respectively).

Accurate codes are desirable because of the high cost of beam time at accelerators that can produce particles with charge and velocity that simulate cosmic rays. They are currently used for a variety of engineering and analysis applications, but full validation for very specialized tasks is still ongoing. If codes are determined to accurately represent physical phenomena then significant "pre-engineering" can be done before experimental work, therefore reducing experimental costs and/or allowing for more efficient use of often limited experimental time.

CHAPTER II

BACKGROUND

Microdosimetric Quantities

In the field of microdosimetry, care must be taken to ensure energy deposition events are characterized properly. The common health physics values of absorbed dose and dose equivalent, while perfectly applicable and widely used for large site sizes, do not carry the same relevance when applied to small volume (i.e. 1 µm site sizes). On the large scale, these average values are sufficient for most applications. On the small scale, however, they do no accurately describe energy deposition. The stochastic nature of energy deposition events becomes increasingly more evident as the site size is reduced until a point is reached where the average values no longer accurately describe the physical phenomena. At this point, energy deposition events are best described by a Poisson distribution.

Microdosimetry is the study of energy deposition in very small volumes. To aide in this study, small volumes are simulated by larger physical volumes. Therefore, a 1 µm site size of unit density (1 g cm^{-3}) can be simulated by a volume orders of magnitude greater in physical dimension, to a size that is much easier to work with. This is done by maintaining the same mass thickness, measured in units of g cm^{-2}, in the simulated volume. This simple relationship is given in Equation (1):

$$(\rho dx)_1 = (\rho dx)_2 \tag{1}$$

where ρ_1 and dx_1 are the density and simulated site size, respectively, and ρ_2 and dx_2 are the density and size of physical site, respectively. For the common site size of 1 µm, ρ_1 would be equal to 1 g cm^{-3} and dx_1 would be equal to 1 µm. Therefore, ρ_2 and dx_2 are chosen such that their product equals the product of ρ_1 and dx_1, 1 x 10^{-4} g cm^{-2}.

There are several stochastic energy deposition quantities of interest in microdosimetry. The first quantity of interest is energy deposition

$$\varepsilon_i = E_{in} - E_{ou} + Q \tag{2}$$

where E_{in} is the energy of the incident ionizing particle (excluding rest energy), E_{out} is the sum of the energies of all ionizing particles leaving the interaction (excluding rest energy) and Q is the change in rest energies of the nucleus and of all particles involved in the interaction. A quantity similar to this is energy imparted

$$\varepsilon = \sum_i \varepsilon_i \tag{3}$$

which is the sum of all energy deposits, ε_i, in a given volume (ICRU 1998).

Next, specific energy, z, is

$$z = \frac{\varepsilon}{m} \tag{4}$$

where ε is the energy imparted by a *single* event and m is the mass of the site giving units of J kg^{-1}. Likewise, the lineal energy, y, is

$$y = \frac{\varepsilon}{\bar{l}} \tag{5}$$

where ε again is the energy imparted by a single event and $\bar{l}$ is the mean chord length of the volume defined as

$$\bar{l} = \frac{4V}{S} \tag{6}$$

by Cauchy's theorem (Cauchy 1908) where V and S are the volume and surface area of the site, respectively. Applying this to a sphere, Equation (6) becomes

$$\bar{l} = \frac{4V}{S} = \frac{4\left(\frac{4}{3}\pi r^3\right)}{4\pi r^2} = \frac{4r}{3} = \frac{2(2r)}{3} = \frac{2D}{3} \tag{7}$$

where r is the radius of the sphere and D is the diameter of the sphere. Likewise, Equation (6) applied to a cylinder becomes

$$\bar{l} = \frac{2DH}{D+2H} \tag{8}$$

where D is the diameter of the cylinder and H is the height.

The units of y are J m^{-1} but the units of keV μm^{-1} are commonly used instead. It is customary to represent single-event distributions as a function of lineal energy, y, rather than specific energy, z (Rossi 1996). As a result, a relationship has been derived that expresses z as a function of y for a spherical site

$$z = \frac{0.204\,y}{(2r)^2} \tag{9}$$

where, again, r is the radius of the spherical site. Using input values of y in units of keV μm^{-1} and r in units of μm, z is given in units of Gy (J kg^{-1}).

When analyzing microdosimetry data, it is often customary to consider the first and second moment of the y distribution, y_F and y_D, respectively,

$$y_F = \int_0^\infty y f(y) dy \tag{10}$$

and

$$y_D = \frac{1}{y_F}\int_0^\infty y^2 f(y)dy \tag{11}$$

where $f(y)$ is the frequency distribution of y. Likewise, the first and second moment of the z distribution are represented by z_F and z_D where

$$z_F = \int_0^\infty z f_1(z)dz \tag{12}$$

and

$$z_D = \frac{1}{z_F}\int_0^\infty z^2 f_1(z)dz \tag{13}$$

where $f_1(z)$ is the frequency distribution of z.

It should be noted that $f_1(z)$ denotes a *single-event* quantity while $f(z)$ represents a general (multi-event) quantity (Rossi 1996).

Stopping Power and Continuous Slowing Down Approximation (CSDA)

Charged-particle Coulomb-force interactions can be classified by the relationship between the classical impact parameter, *b*, and the atomic radius, *a* (Attix 1986). The three classifications are "soft" collisions (b>>a), hard (or "knock-on") collisions (b ~ a), and Coulomb-force interactions with the external nuclear field (b<<a). The interaction of interest in this study is the hard collision (b ~ a) because of the delta ray production (since the goal of this study is to study how well FLUKA can simulate a TEPC and produce the expected delta ray events).

The rate of energy loss per unit path length by the incident particle is known as the stopping power and denoted as $\frac{dT}{dx}$ which has SI units of J m-^{1} and common units of keV μm^{-1}. If stopping power is divided by density (in effect normalizing it for all densities), it is know as the mass stopping power. Ignoring radiative stopping power, the collision stopping power becomes the total stopping power:

$$\left(\frac{dT}{\rho dx}\right)_c = \left(\frac{dT_s}{\rho dx}\right)_c + \left(\frac{dT_h}{\rho dx}\right)_c \tag{14}$$

where the subscript *s* denotes soft collisions and *h* denotes hard collisions (the collision of interest) and the subscript *c* denotes collision (as opposed to radiative).

The maximum energy that can be transferred to an atomic electron in a hard collision (and therefore the maximum energy of a delta ray) is denoted by $T'_{\max}$

$$T'_{\max} \cong 2m_o c^2\left(\frac{\beta^2}{1-\beta^2}\right) = 1.022\left(\frac{\beta^2}{1-\beta^2}\right)\text{MeV} \tag{15}$$

where β is defined as

$$\beta = \frac{v}{c}. \tag{16}$$

The relationship between *T*, kinetic energy, and β is described by

$$T = M_o c^2\left[\frac{1}{\sqrt{1-\beta^2}} - 1\right] \tag{17}$$

where $M_o c^2$ is the rest mass energy of the incident particle. As Equation (17) demonstrates, the kinetic energy required by any particle to reach a given velocity is proportional to its rest energy. Rearranging Equation (17) gives

$$\beta = \left[1 - \left(\frac{1}{(T / M_o c^2) + 1} \right)^2 \right]^{1/2} . \tag{18}$$

Equation (14) can be expanded (Attix 1986) for heavy particles to give

$$\left(\frac{dT}{\rho dx} \right)_c = 0.3071 \frac{Z z^2}{A \beta^2} \left[13.8373 + \ln \left(\frac{\beta^2}{1 - \beta^2} \right) - \beta^2 - \ln I \right] \tag{19}$$

where Z and A are the atomic number and mass number of the stopping medium, respectively, z is the charge of the incident particle and I is the mean excitation potential of the struck atom. Equation (19) modified to include a shell correction term that takes into account the relative participation of atomic electrons in the slowing down process as the incident particle slows down:

$$\left(\frac{dT}{\rho dx} \right)_c = 0.3071 \frac{Z z^2}{A \beta^2} \left[13.8373 + \ln \left(\frac{\beta^2}{1 - \beta^2} \right) - \beta^2 - \ln I - \frac{C}{Z} \right] . \tag{20}$$

This impact of this correction term is insignificant for the incident particle energies discussed in this paper. Nonetheless, it is included for completeness.

Similarly, Equation (14) can be expanded for electrons and positrons:

$$\left(\frac{dT}{\rho dx} \right)_c = k \left[\ln \left(\frac{\tau^2 (\tau + 2)}{2(I / m_o c^2)} \right) + F^{\pm}(\tau) - \delta - \frac{2C}{Z} \right] \tag{21}$$

where

$$\tau \equiv \frac{T}{m_0 c^2} , \tag{22}$$

for electrons

$$F^{-}(\tau) \equiv 1-\beta^2+\frac{\tau^2/8-(2\tau+1)\ln 2}{(\tau+1)^2}, \tag{23}$$

for positrons

$$F^{+}(\tau) \equiv 2\ln 2-\frac{\beta^2}{12}\left\{23+\frac{14}{\tau+2}+\frac{10}{(\tau+2)^2}+\frac{4}{(\tau+2)^3}\right\}, \tag{24}$$

δ is the correction term for the density effect and *C/Z* is the previously discussed shell correction term. In the case where the stopping medium is a mixture of elements, the stopping power of the mixture is represented by the weighted sum of the stopping powers of the composing materials according to Bragg's Rule (ICRU 1984):

$$\left(\frac{dT}{\rho dx}\right)_{mix} = f_{z_1}\left(\frac{dT}{\rho dx}\right)_{z_1} + f_{z_2}\left(\frac{dT}{\rho dx}\right)_{z_2} + \ldots \tag{25}$$

Similarly, δ for a mixture is

$$\delta = \frac{\sum_i f_{z_i}(Z/A)_i \delta_i}{Z/A}. \tag{26}$$

Another quantity of interest is the restricted stopping power which is the fraction of the collision stopping power that includes all soft collisions and those hard collisions resulting in delta rays with energies less than the cutoff value Δ (Attix 1986). If Δ is increased to equal $T'_{\max}$ (given in Equation (15)), then

$$\left(\frac{dT}{\rho dx}\right)_{\Delta} = \left(\frac{dT}{\rho dx}\right)_{c}. \tag{27}$$

For electrons and positrons this quantity is

$$\left(\frac{dT}{\rho dx}\right)_{\Delta} = k\left\{\ln\left[\frac{\tau^2(\tau+2)}{2(I/m_o c^2)^2}\right] + G^{\pm}(\tau,\eta) - \delta - \frac{2C}{Z}\right\} \tag{28}$$

where

$$\eta \equiv \frac{\Delta}{T}, \tag{29}$$

for electrons

$$G^{-}(\tau,\eta) = -1-\beta^2 + \ln\left[4(1-\eta)\eta\right] + (1-\eta)^{-1} + (1-\beta^2)\left[\tau^2\eta^2/2 + (2\tau+1)\ln(1-\eta)\right] \tag{30}$$

and for positrons

$$G^{+}(\tau,\eta) = \ln 4\eta - \beta^2\begin{bmatrix}1+(2-\zeta^2)\eta-(3+\zeta^2)(\zeta\tau/2)\eta^2\\ +(1+\zeta\tau)(\zeta^2\tau^2/3)\eta^3-(\zeta^3\tau^3/4)\eta^4\end{bmatrix}, \tag{31}$$

where

$$\xi \equiv (\tau+2)^{-1}. \tag{32}$$

Finally, the range of a charged particle is the expectation value of the pathlength *p* that is follows until it comes to rest which defined as

$$\Re_{\mathrm{CSDA}} \equiv \int_0^{T_0}\left(\frac{dT}{\rho dx}\right)^{-1} dT \tag{33}$$

where T_0 is the starting energy of the particle. If $dT/\rho dx$ is in MeV cm^2/g and dT in MeV, then $\Re_{\mathrm{CSDA}}$ is thus given in g cm^{-2} (Attix 1986). Because of the complexity of the stopping power equations, they and $\Re_{\mathrm{CSDA}}$ are often found from tabulated references. The $\Re_{\mathrm{CSDA}}$ for a heavy charged particle of charge *z* and rest mass M_0 can be found via tabulated proton data by the relationship

$$\Re_{\mathrm{CSDA}} = \frac{\Re^{P}_{\mathrm{CSDA}} M_0}{M_0^{P} z^2} \tag{34}$$

where $\Re^{P}_{\mathrm{CSDA}}$ is the range of a proton of rest mass M_0^{P}.

Tissue-Equivalent Proportional Counter

A tissue-equivalent proportional counter (TEPC) is a specialized type of proportional counter whose wall and fill gas mimic the elemental composition of biological tissue (Knoll 2000). It is a versatile dosimeter because can measure both absorbed dose and dose equivalent in a mixed radiation field. For walls that are sufficiently thick compared to the range of delta rays produced in the wall, an equilibrium exists whereby the flux of delta rays entering the gas volume becomes independent of the wall thickness (this phenomenon will be exploited later). In the case of a low pressure TEPC, direct measurement of energy imparted, ε from Equation (3), is possible on an event by event basis. In summary, proportional counters are the principal instruments of microdosimetry (Rossi 1996).

FLUKA

The objective of this study is to determine how well the Monte Carlo transport code FLUKA (Fasso 2005) can simulate a TEPC and produce the expected delta ray events. FLUKA is the code of choice for this research because of its ability to simulate about 60 different particles, including electrons from 1 keV to thousands of TeV and

hadrons of energies up to 20 TeV (Fasso 2005). For this application, FLUKA is a very flexible code.

FLUKA is a general purpose Monte Carlo code for the interaction and transport of hadrons, heavy ions, and electromagnetic particles from few keV (or thermal energies for neutrons) to cosmic ray energies in whichever material (Battistoni 2007).

As in most simulation codes that adopt a "condensed history" approach, in FLUKA "continuous" processes such as energy loss and angular deflections due to Coulomb interactions and "discrete" processes (delta ray production, nuclear interactions, decays, bremsstrahlung and photon interaction) are treated separately (Fasso 2005).

The FLUKA code was originally developed in 1962 by J. Ranft and H. Geibel, who initiated the code for hadron beams. The name FLUKA (from FLUktuierende KAscade) came in 1970. Between 1970 and 1987 the development of the code was carried out in the framework of a collaboration between CERN and the groups of Leipzig and Helsinki. That version was essentially for shielding calculations.

Since 1989 FLUKA has been developed within INFN (National Institute of Nuclear Physics) with the personal collaboration of A. Fassò (CERN) and J. Ranft (Leipzig).

In 1990 MCNPX officially started using FLUKA for its high energy part. In 1993 FLUKA was interfaced to GEANT3 (for the hadronic part only). This interface did not follow the subsequent FLUKA developments and it is therefore now obsolete.

Since 2002, FLUKA is an INFN project. The INFN project is carried on in collaboration with CERN and the University of Houston (Fasso 2005).

According to the FLUKA manual, delta ray production is controlled via Bhabha and Møller scattering (Fasso 2005). As previously mentioned (and will be seen in the results), delta ray production greatly influences the response of a TEPC. Specifically, the two phenomena of interest are delta ray production in the wall and delta ray escape from the gas to the wall. Simulating the response of a TEPC would be very difficult if not impossible without an accurate model for delta ray production.

FLUKA's most current transport limits appear in Table 1.

Table 1 – FLUKA transport limits (Fasso 2005)

	Secondary particles	Primary particles
charged hadrons	1 keV–20 TeV (a)	100 keV–20 TeV (a)
neutrons	thermal–20 TeV (a)	thermal–20 TeV (a)
antineutrons	1 keV–20 TeV (a)	10 MeV–20 TeV (a)
muons	1 keV–1000 TeV	100 keV–1000 TeV
electrons	1 keV–1000 TeV	70 keV–1000 TeV (low-Z materials) 150 keV–1000 TeV (high-Z materials)
photons	1 keV–1000 TeV	7 keV–1000 TeV
heavy ions	10 MeV/n–10000 TeV/n	100 MeV/n–10000 TeV/n

(a) 10 PeV with the Dpmjet interface

CHAPTER III

METHODS

General Considerations

A TEPC was constructed according to the experimental specifications (Gersey 2002) which simulated a 1 µm site size of unity density (1 g cm $^{-3}$). This included a spherical gas volume 1.27 cm in diameter with a 0.254 cm thick tissue-equivalent (TE) wall. Gersey states a gas pressure of 33 torr was used which corresponded to a 1 µm site size. A simple calculation was performed using Equation (1) that gave a necessary gas density to produce a 1 µm site size of 7.87×10^{-5} g cm^{-3}.

Propane (C_3H_8) was used as the fill gas. The composition of the TE material used was not detailed. Therefore, it was assumed to be A-150 tissue-equivalent plastic as per the NIST standard with a density of 1.127 g cm^{-3} (NIST 2010). A-150's composition is detailed in Table 2. As a side note, FLUKA does not have fluorine listed as one of its standard materials. A separate material declaration was needed to create fluorine.

Table 2 – Composition of A-150 tissue-equivalent plastic

Atomic number	Fraction by weight
1	0.101327
6	0.775501
7	0.035057
8	0.052316
9	0.017422
20	0.018378

All FLUKA simulations were run with the TEPC in a vacuum. Gersey did not give specifications of the anode. As a result, a 45 μm diameter tungsten anode was constructed in the FLUKA input file. The simulated TEPC consisted of five regions as detailed in Table 3.

Table 3 – FLUKA regions of simulated TEPC

Region number	Description
1	Blackhole/universe
2	Vacuum
3	A-150 tissue-equivalent wall
4	Gas volume, C_3H_8
5	Tungsten anode

Both electron transport limit and delta ray production thresholds were set to 1 keV. Both of these limits were applied to all materials. FLUKA SCORE commands 208, deposited energy (FLUKA name "Energy"), and 211, electromagnetic energy (electrons, positrons or photons – FLUKA name "EM-ENRGY") were used for all runs. Essentially, 208 gives energy deposition from primary plus delta rays while 211 gives just energy deposition from delta rays because FLUKA was set not to transport photons by using the DISCARD command. Data were generated using the EVENTDAT card which tabulated requested values (in this case 208 and 211) for each region. A small C++ program was used to extract the relevant data from the FLUKA output file.

FLUKA was run on the Texas A&M Department of Nuclear Engineering Unix cluster, grove, the specifications for which appear in Table 4.

Table 4 – grove specifications

Server name	Server type	Processor specifications	Operating system	RAM
grove	Dell PowerEdge 2950 (master)	(2) Intel Xeon 5345 (Quad-Core 2.33GHz)	RedHat Enterprise Linux AS 4	16GB
compute-00 through compute -09	Dell PowerEdge 1950 (10 nodes)	(2) Intel Xeon 5345 (Quad-Core 2.33GHz) each 80 processor equivalent for running jobs	RedHat Enterprise Linux WS 4	20GB

Beam Geometry

The simulation consisted of passing an ^{56}Fe beam at 360 MeV/nucleon through the detector, perpendicular to the axis of the anode. In all cases, the beam started 2 cm outside the TEPC and energy deposition was recorded (via SCORE 208 and/or SCORE 211) in the gas only (FLUKA region 4).

Four specific beam profiles were run:

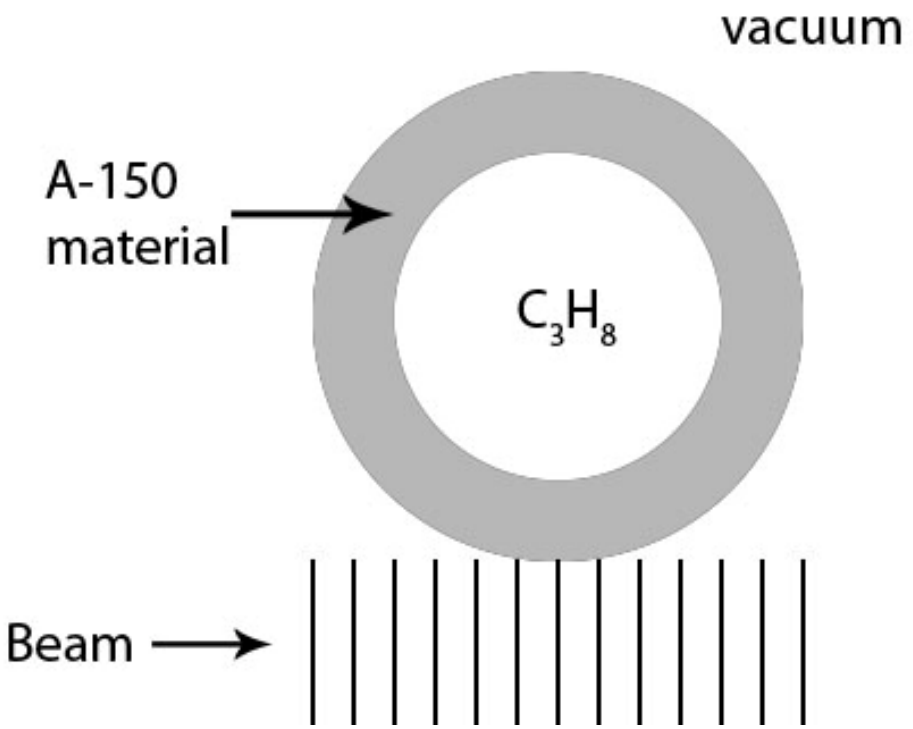

Figure 1 – Beam schematic a broad beam. The broad beam has the shape of an annular ring with inner radius = 0 and outer radius = detector radius.

a uniform broad beam covering the entire cross sectional area of the detector (Fig. 1),

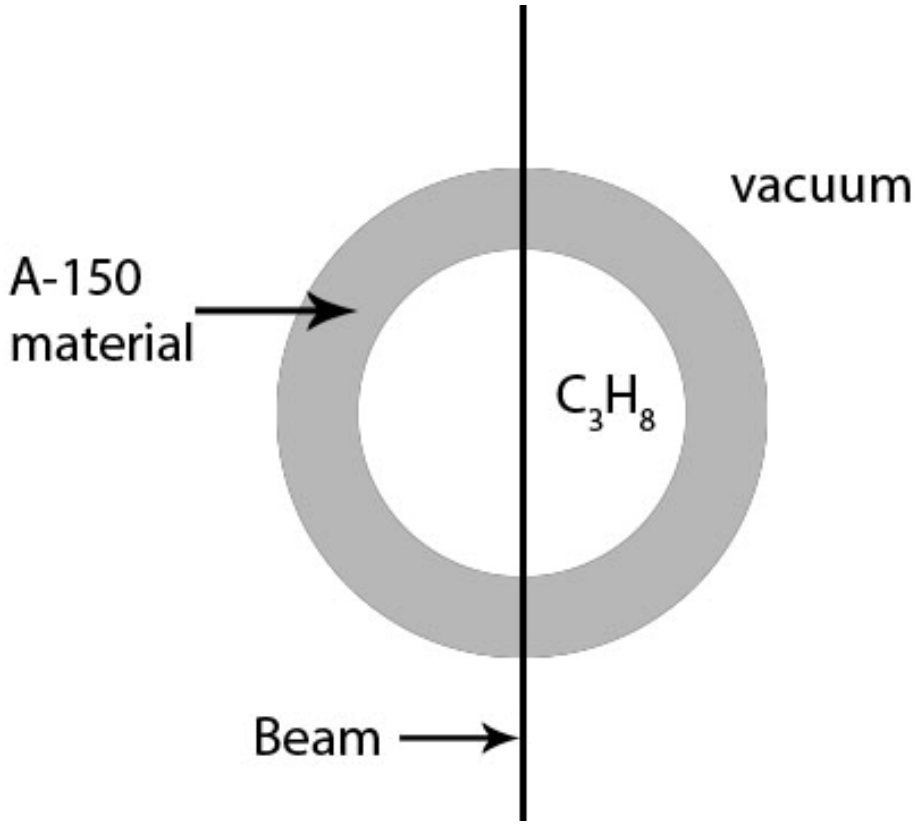

Figure 2 – Beam schematic for a narrow beam down the diameter.

a narrow beam down the diameter of the detector (Fig. 2),

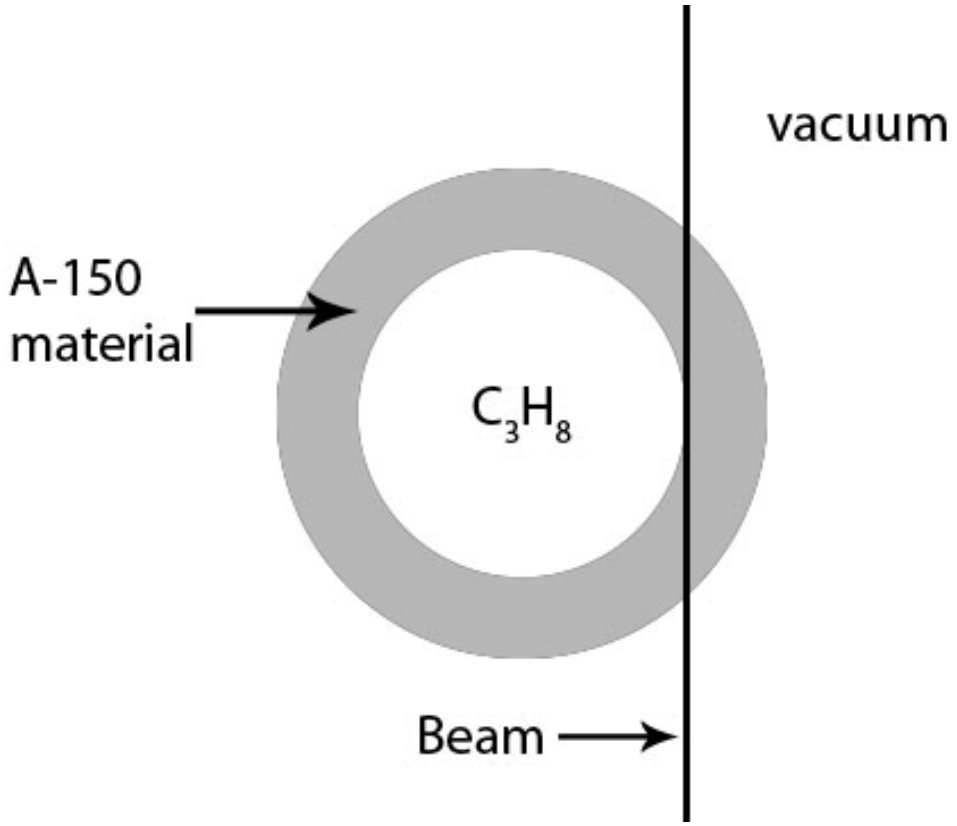

Figure 3 – Beam schematic for a narrow beam 1 μm inside the gas/wall interface

a narrow beam 1 μm inside the gas/wall interface (Fig. 3),

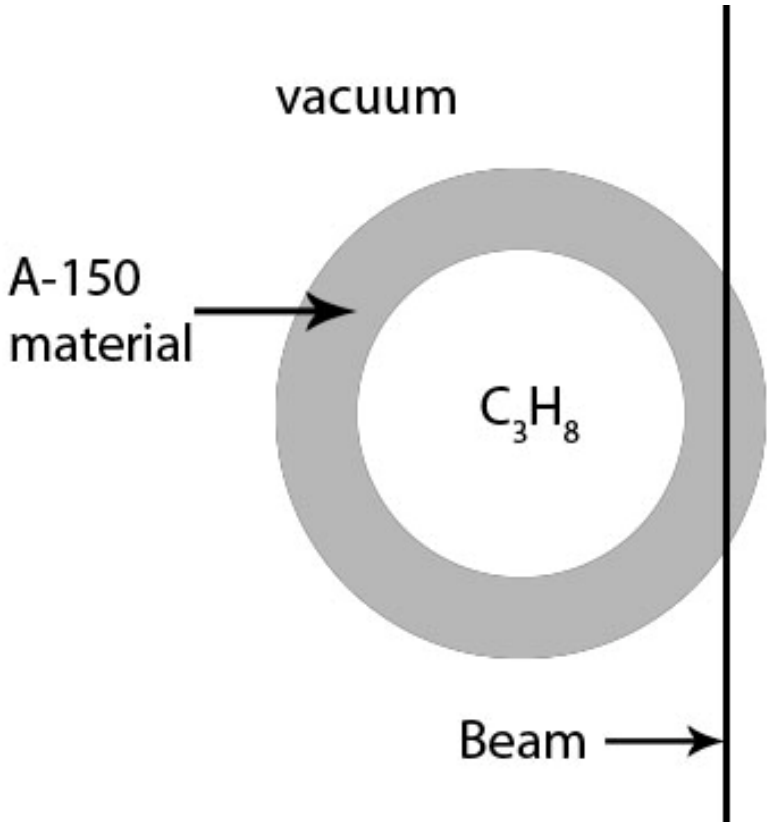

Figure 4 – Beam schematic for a narrow beam 1000 µm inside the gas/wall interface.

and a narrow beam 1000 µm inside the gas/wall interface (Fig. 4). The latter three narrow beams are meant to provide insight into explaining and characterizing how energy enters and is lost due to the inhomogeneous gas/wall interface, better explaining the features of the broad beam. Each beam orientation was run with and without FLUKA transporting delta rays. This was done to show that when delta rays are "turned off," FLUKA deposits energy locally.

In addition, a series of narrow beams were ran a varying impact parameters (radial distance from center of detector to beam axis) to further explore the effect of the TE wall on the delta ray spectrum. The beams were kept uniform (^{56}Fe at 360 MeV/nucleon) and only the beam location was changed. In a similar fashion, the beam location was held constant (impact parameter < 0.5 mm) while the beam energy was varied (200-1000 MeV/nucleon ^{56}Fe) to verify FLUKA's scoring of energy deposition of beam of varying LET.

Wall Thickness

Because of the long runtimes of these simulations, anywhere from 10-20 days to produce statistically acceptable results for beam orientations described in Figs. 1-4, the option of using a thinner wall was explored. To find an acceptable thinner wall, energy deposition from electrons, specifically delta rays, only (SCORE 211 from above) was used. The first test consisted of performing the run detailed in Fig. 2, 360 MeV/nucleon ^{56}Fe narrow beam down the diameter, except with a varying TE wall thickness. From these data, it was expected to find that the energy deposition will plateau and further increasing the wall thickness will have no effect on the energy deposition. The goal of this test is to find the range of forward-going delta rays produced in the wall.

In a second test, the standard beam, 360 MeV/nucleon ^{56}Fe, was passed down the axis of a 1 µm long, 1000 µm radius TE cylinder. Energy deposition from electrons was scored as a function of radial distance from 100 to 1000 µm in 25 µm increments. Similar to the goal of the first test, the goal of this test is to find the range of delta rays in

the radial direction. To find the range of delta rays in angles between 0 and 90º, this test was repeated for a 1000 µm long, 1000 µm radius TE cylinder.

CHAPTER IV

RESULTS AND DISCUSSION

Simulated TEPC

The first data set of interest is the energy deposition histogram for an evenly distributed broad beam incident on the simulated TEPC shown in Fig. 5. This response is what is typical for a detector with a solid wall exposed to a radiation source in a laboratory.

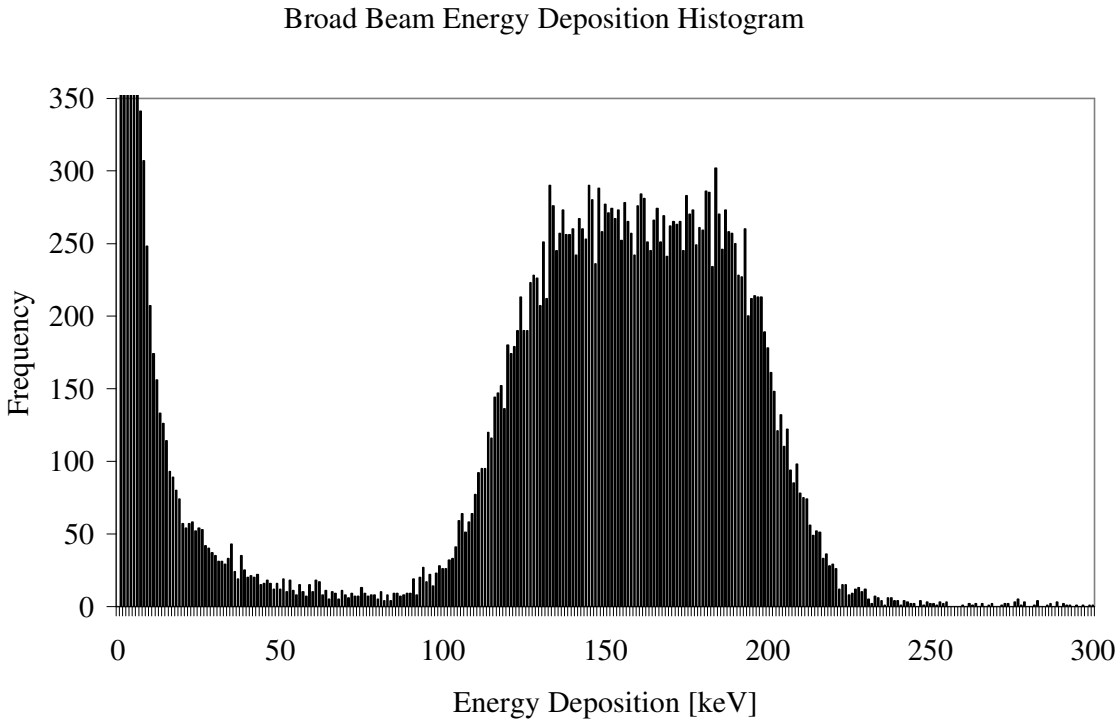

Figure 5 – Energy Deposition Histogram for an ^{56}Fe beam at 360 MeV/nucleon incident on the simulated TEPC (broad beam, covering entire surface area)

In the paper detailing the experimental data, the three general energy regions of this plot were identified – low energies (< 10 keV), peak at mid energies, and the small number of very high energy events. To explain these regions of interest, the broad beam plot in Fig. 5 will be compared to the three specific narrow beams outlined in Figs. 2-4.

The first narrow beam of interest is that of a narrow beam passed down the diameter of the detector, perpendicular to the anode. The resulting energy deposition histogram is shown in Fig. 6. The beam orientation was matched to the beam in the experimental data, all particles having an impact parameter less than 0.5 mm (Gersey 2002). This narrow beam is responsible for the peak and most probable energy deposition value of ~200 keV found in Fig. 5.

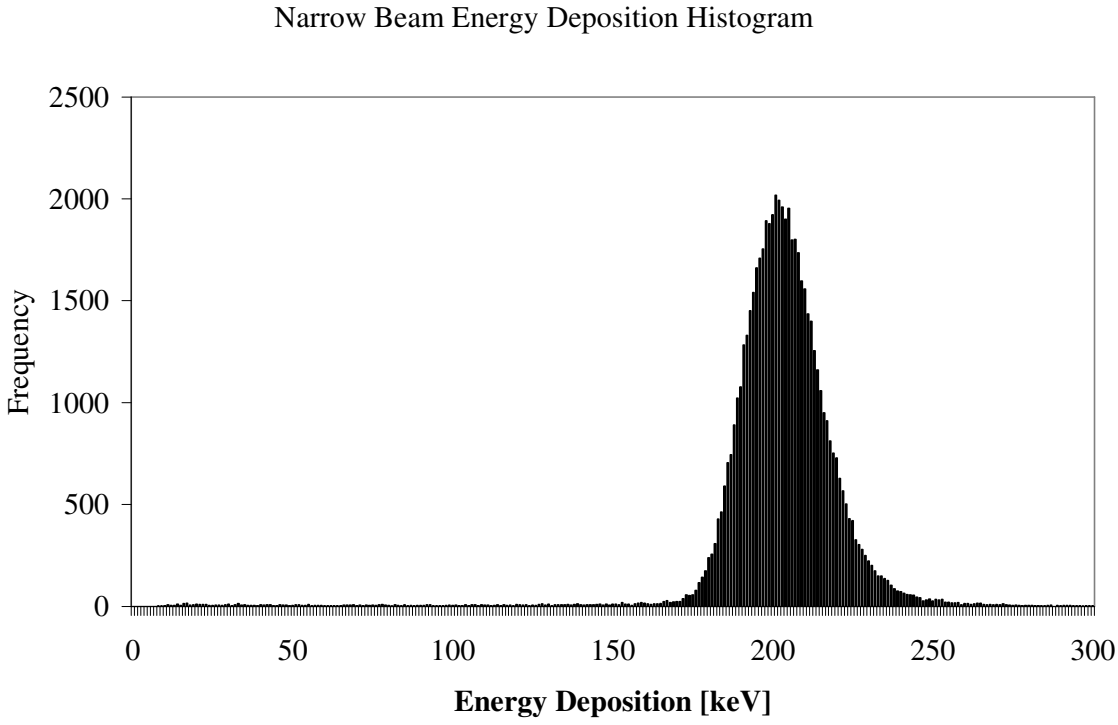

Figure 6 – Energy Deposition Histogram for an ^{56}Fe beam at 360 MeV/nucleon with an impact parameter less than 0.5 mm incident on the simulated TEPC.

The second narrow beam of interest is that passed almost tangent to the gas/wall interface (specifically 1 μm inside the TE wall). This spectrum has two general features worth noting. First, this spectrum is quite broad. The histogram in Fig. 7 shows values out to 1000 keV. However, this represents a truncation of the entire spectrum with recorded events well past the 1000 keV cutoff. The second point of interest is that the average energy deposition of this spectrum is much greater than that of the other spectra. As evident from this spectrum, beams tangent (or close to tangent) to the gas/wall interface are responsible for the highest energy deposition events found in the broad

beam. Additionally, because of the broad spectrum produced by a tangent beam, it can be said that the broadness of the tangent beam spectrum, generally speaking, "washes out" the broad beam spectrum a bit making details less pronounced than in other spectra.

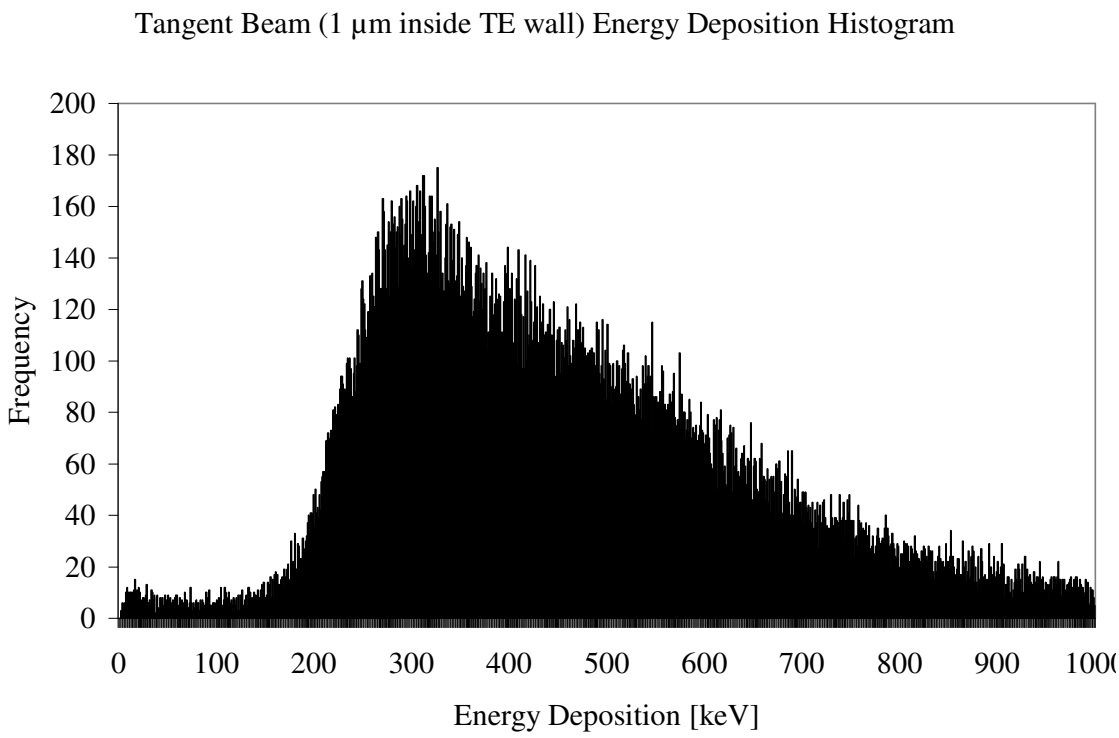

Figure 7 – Energy Deposition Histogram for a tangent (1 µm inside the gas/wall interface) ^{56}Fe beam at 360 MeV/nucleon incident on the simulated TEPC.

The third and final narrow beam of interest is that passed 1000 µm inside the gas/wall interface. As evident in the histogram in Fig. 8, this beam orientation is responsible for the very low energy deposition events in the simulated TEPC. The energy deposition is so low because all delta rays produced in the wall by the incident

beam have to travel through at least 1000 µm of TE material before they reach the gas. In many cases, this was enough material to stop the delta rays completely resulting in zero energy deposition in the gas. For the delta rays that did make it through the TE wall and into the gas, very little energy (a few keV) was deposited.

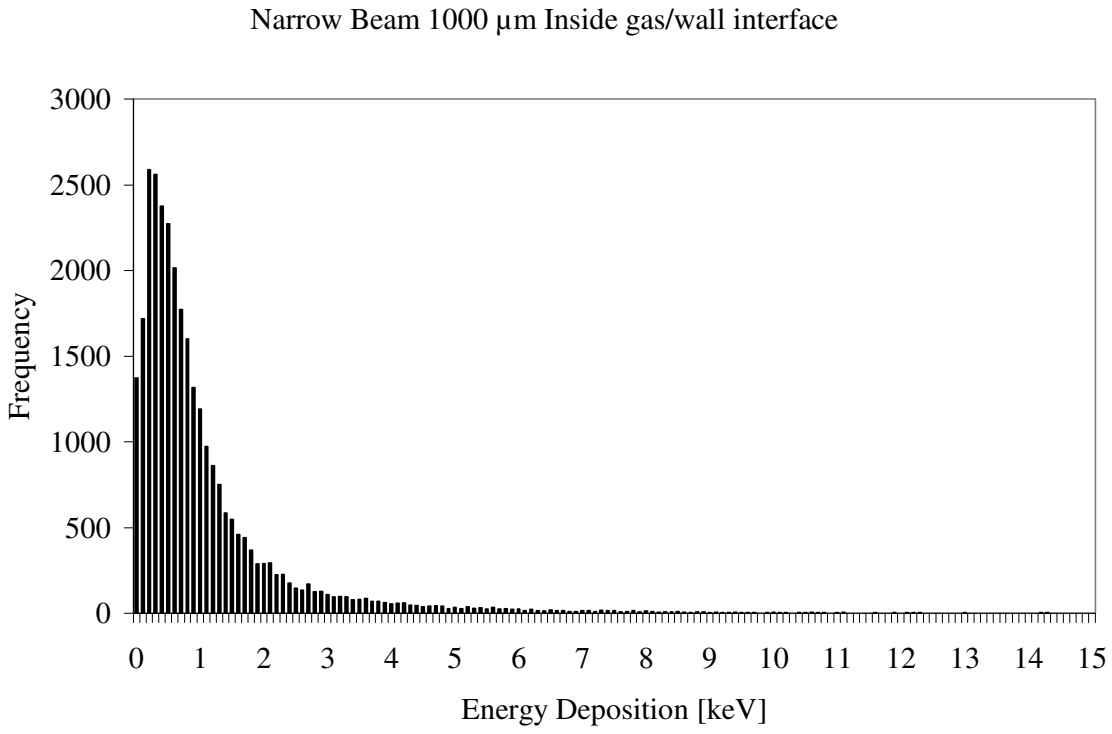

Figure 8 – Energy Deposition Histogram for a narrow ^{56}Fe beam at 360 MeV/nucleon 1000 µm inside the gas/wall interface incident on the simulated TEPC.

With the features of the broad beam explained by narrow beams, the next step in analyzing how well FLUKA produces the expected delta ray events is to explore what happens when delta rays are turned off in FLUKA (i.e. the DELTARAY command is not

included in the input file). To conduct this study, the same input file used to generate the histogram in Fig. 6 (narrow beam with impact parameter < 0.5 mm) was used except that the DELTARAY command was commented out. The resulting energy deposition histogram is in Fig. 9. A comparison of Figs. 6 and 9 (delta rays "on" and "off") show they both contain a peak and most probable value at ~200 keV. However, with delta rays off, the distribution has a large tail that extends out well past the 300 keV cutoff of the plot window. This large tail is present because with delta rays turned off, FLUKA is depositing all energy locally. That is, where delta rays would normally carry a significant fraction out of the gas and into the wall, FLUKA is now depositing all of the delta ray's kinetic energy at the location it is produced.

In this case, energy loss by the particle passing through the gas is equal to the energy deposited in the gas. For the case of delta rays turned on, this is not the case and the energy deposited in the gas is less than the energy lost by the incident particle passing through the gas.

This "delta ray off" energy deposition histogram resembles a Vavilovian energy loss distribution (Vavilov 1957).

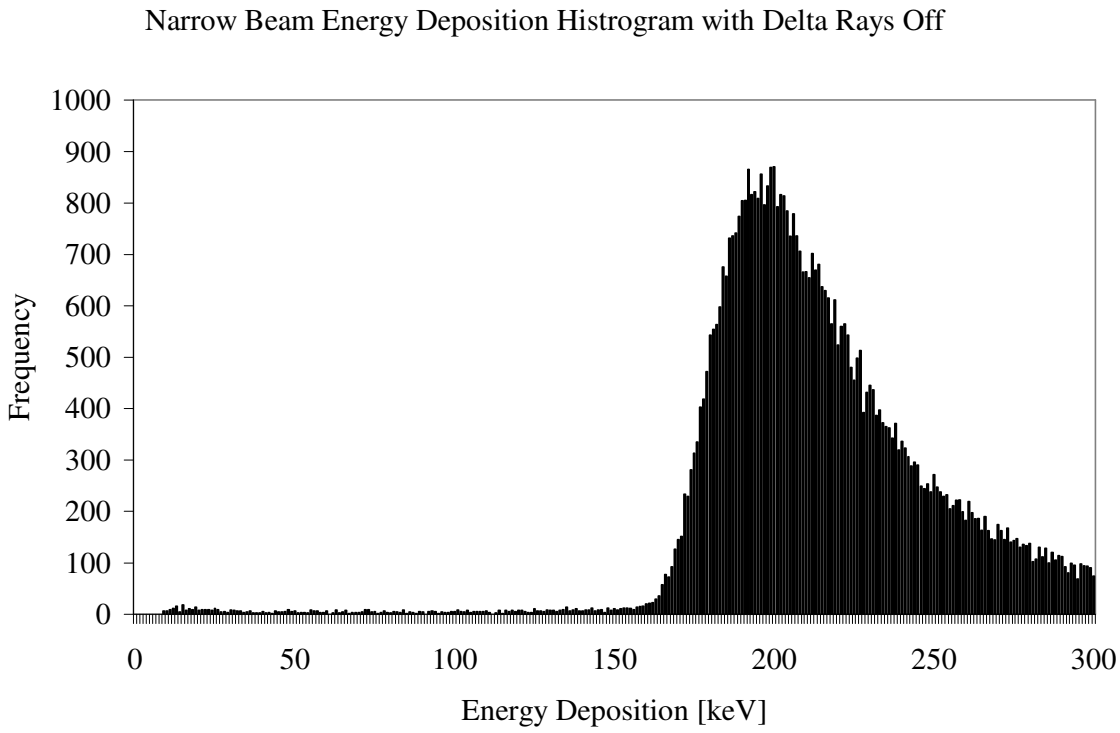

Figure 9 – Energy Deposition Histogram for an ^{56}Fe beam at 360 MeV/nucleon incident on the simulated TEPC (broad beam, covering entire surface area) with delta rays turned off.

Another point of interest for the simulated TEPC is how the TE wall affects the energy deposition spectrum. The energy deposition histogram for a wall-less TEPC (TE wall replaced with a vacuum) with delta rays turned on and the incident beam having an impact parameter less than 0.5 mm is found in Fig. 10. This is the same beam orientation as in Fig. 6 except no detector wall is present. As a comparison shows, the spectra in Figs. 6 and 10 are quite similar. Both contain a very well defined narrow peak with the only difference being the wall-less peak has shifted down about 20 keV as

compared to the walled peak (~180 keV vs. ~200 keV). This spectrum shift is due to the loss of the delta rays entering the gas volume from the TE wall (i.e. the forward-going delta rays). It should be noted again that in all simulations, only energy deposition in the gas was scored. As a result, the energy loss in the wall (or lack of in the case of a wall-less detector) does not affect the energy deposition in gas except for the delta rays produced in the wall that manage to make it to the gas volume.

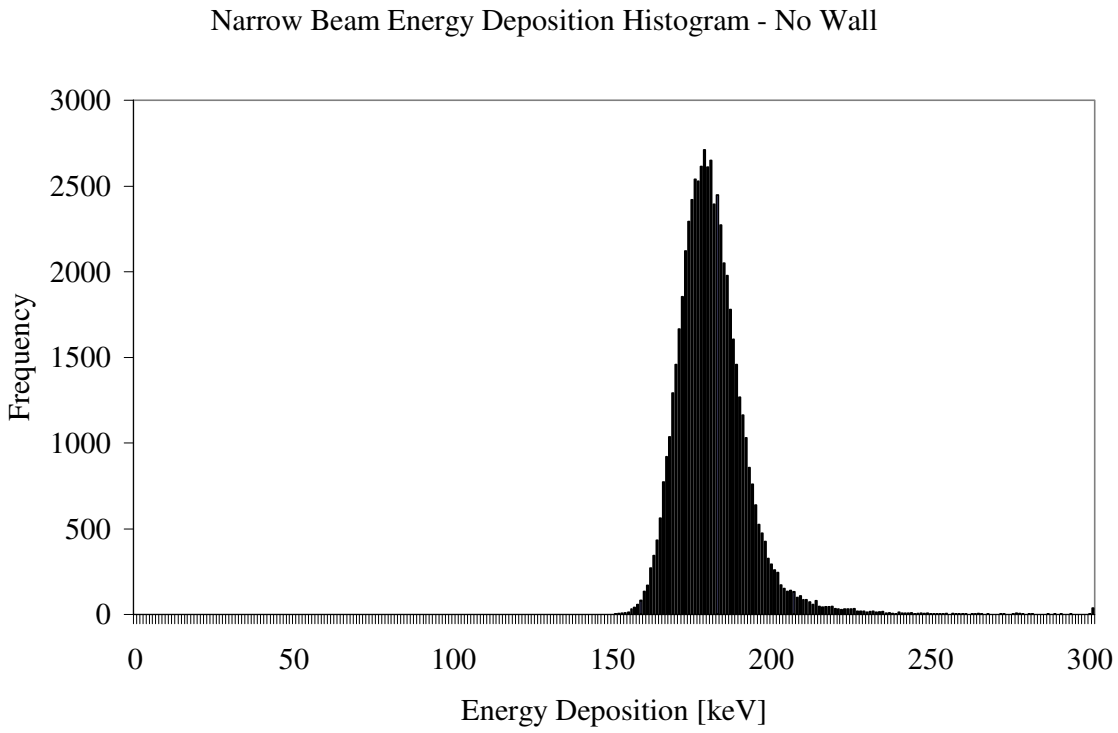

Figure 10 – Energy Deposition Histogram for an ^{56}Fe beam at 360 MeV/nucleon with an impact parameter less than 0.5 mm incident on the simulated TEPC without a wall.

A comparison of the walled and wall-less energy deposition histograms is found in Fig. 11. As stated above, the peak for the wall-less detector has been shifted ~20 keV lower than the walled detector. Additionally, the height of the walled detector distribution is slightly lower than the wall-less distribution. This is because the walled peak is slightly wider than the wall-less peak, most likely due to the variance in the number of delta rays entering the gas.

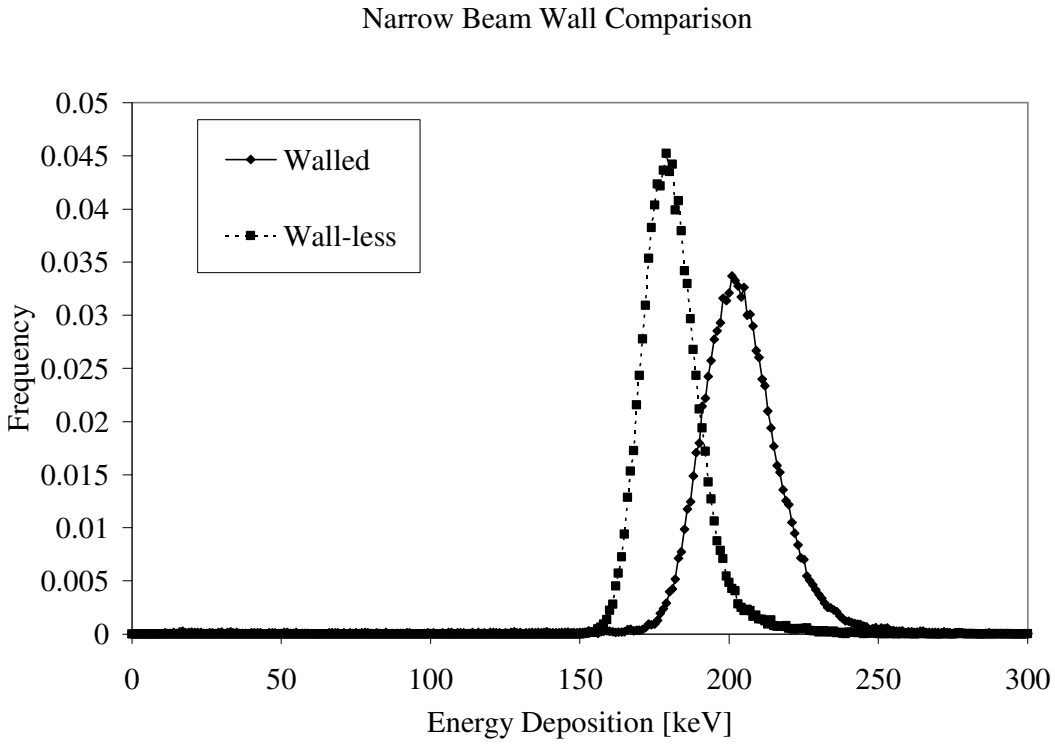

Figure 11 – Comparison of Energy Deposition Histograms for an ^{56}Fe beam at 360 MeV/nucleon with an impact parameter less than 0.5 mm incident on the simulated walled (solid line) and wall-less (dashed line) TEPC.

Wall Thickness/Delta Ray Range

The next area of consideration is how the TE wall thickness affects the energy deposition in the gas. As discussed earlier, the wall is important not because of the energy lost by the primary beam in it but rather the energy deposited in the gas volume by delta rays produced in the wall.

To begin this study, a 1000 µm radius cylinder made of A-150 TE material was simulated as outlined in Chapter III. Energy deposition as a function of radial distance was plotted for a narrow beam passed down the axis of the cylinder as shown in Fig. 12. Since the primary 360 MeV/nucleon ^{56}Fe beam was passed down the axis, the energy deposition at hundreds of µm away from the axis is from the delta rays produced by the primary beam. As expected, energy deposition decreases as the radial distance increases.

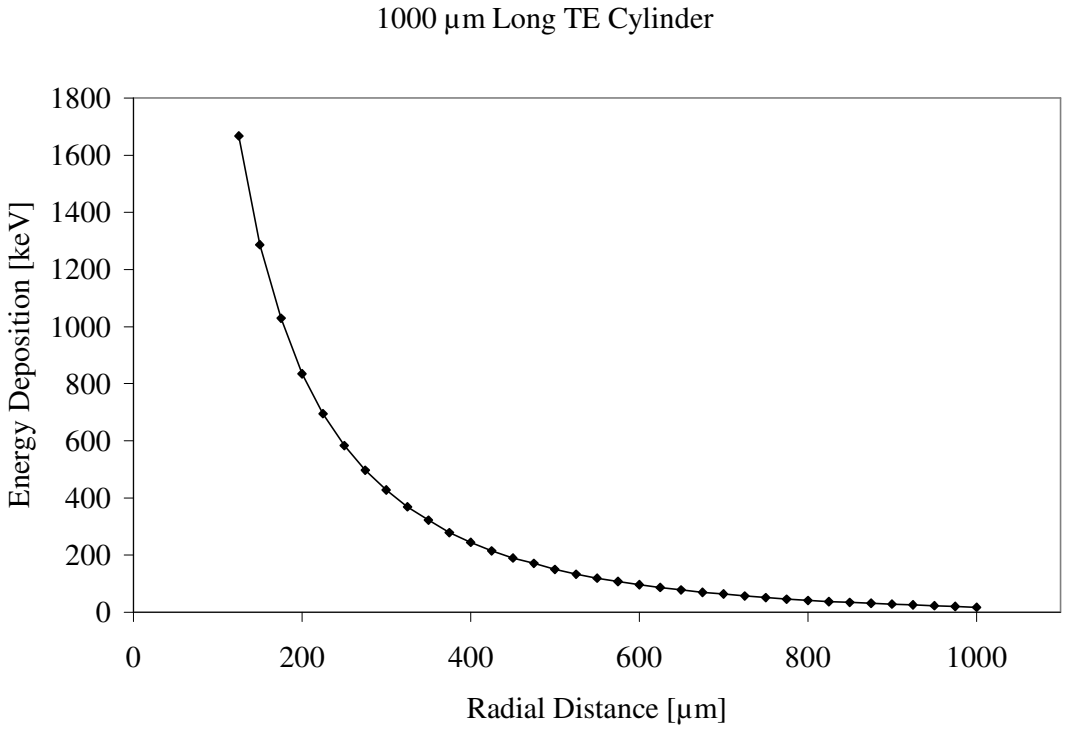

Figure 12 – Energy deposition as a function of radial distance for a narrow ^{56}Fe beam at 360 MeV/nucleon passed down the axis of a 1000 µm long, 1000 µm radius cylinder of TE material on a linear scale.

It should be noted that this geometry is sufficient (i.e. equal length and radius) to record energy deposition for delta rays produced at all angles (as opposed to just in the radial direction to be discussed next).

A plot of the same spectrum appears in Fig. 13 but this time a log scale is used for the y axis to show detail at the larger radial distances. As the plot shows, even at a radial distance of 1000 µm, there is still a non-negligible amount of energy deposition, ~10 keV.

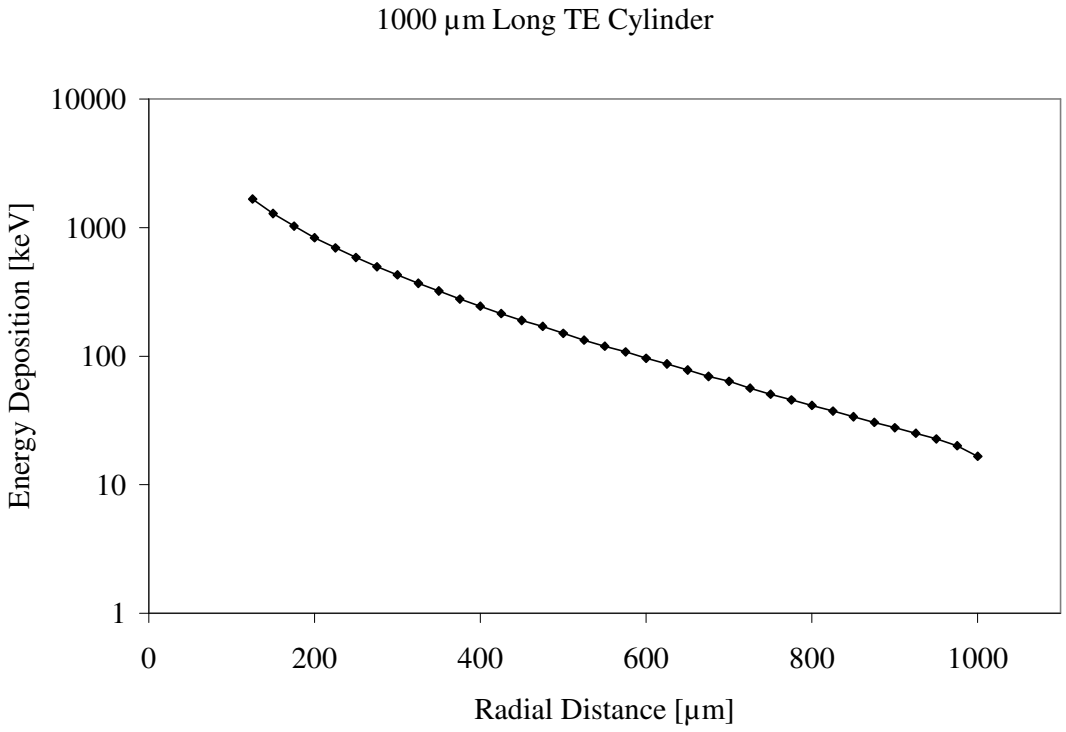

Figure 13 – Energy deposition as a function of radial distance for a narrow ^{56}Fe beam at 360 MeV/nucleon passed down the axis of a 1000 µm long, 1000 µm radius cylinder of TE material on a log scale.

A plot similar to that found in Fig. 12 is found in Fig. 14. However, the TE cylinder in this case is only 1 µm long as opposed to 1000 µm long in Fig. 12. This thin

cylinder (closer in relative dimensions to a coin) is meant to capture only those delta rays produced at an angle of 90 º with respect to the primary beam. The shape is similar, but the magnitude of energy deposition is less (as expected).

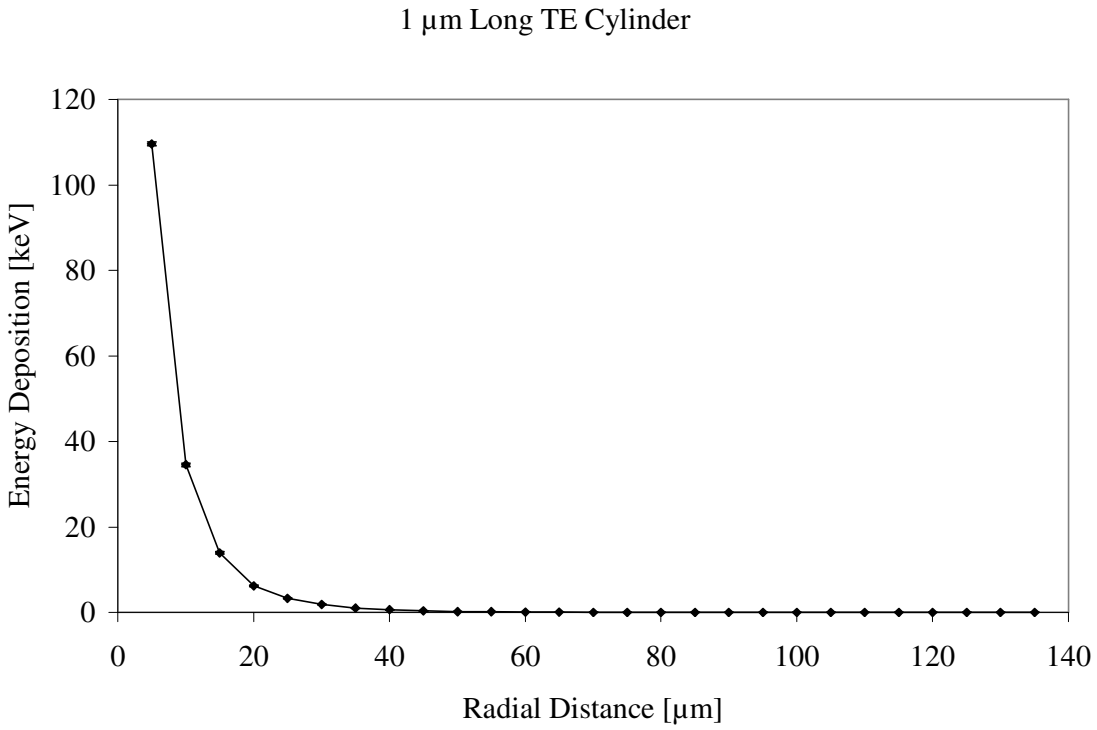

Figure 14 – Energy deposition as a function of radial distance for a narrow ^{56}Fe beam at 360 MeV/nucleon passed down the axis of a 1 µm long, 1000 µm radius cylinder of TE material on a linear scale.

A plot of the same spectrum appears in Fig. 15 but this time a log scale is used for the y axis to show detail at the larger radial distances. As the plot shows, energy deposition is reduced to very small values (on the order of tens of eV) once a radial

distance of 100 µm is reached. It should be noted that as radial distance increases, the 2σ error bars increase as well. Once a radial distance of 120 µm is reached, the 2σ error bars approach an order of magnitude. This is a result of an increasing number of zero energy deposition events as radial distance increases. After about a 100 µm radial distance, a significant fraction of delta rays have stopped in the TE material.

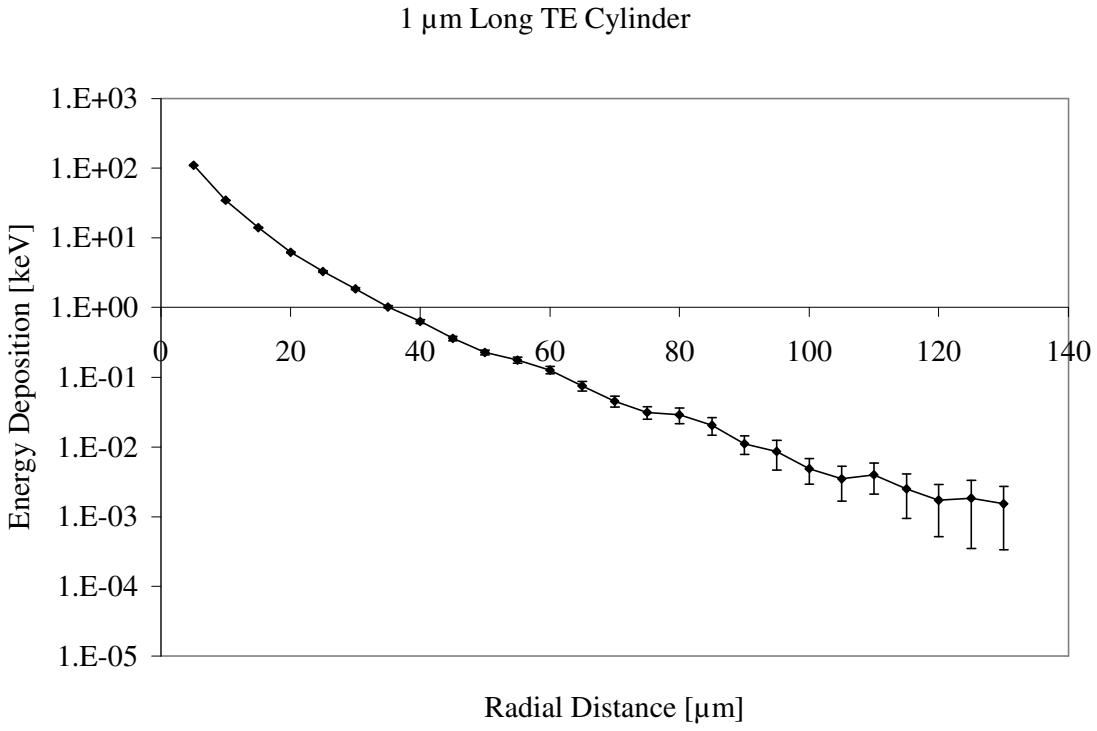

Figure 15 – Energy deposition as a function of radial distance for a narrow ^{56}Fe beam at 360 MeV/nucleon passed down the axis of a 1 µm long, 1000 µm radius cylinder of TE material on a log scale.

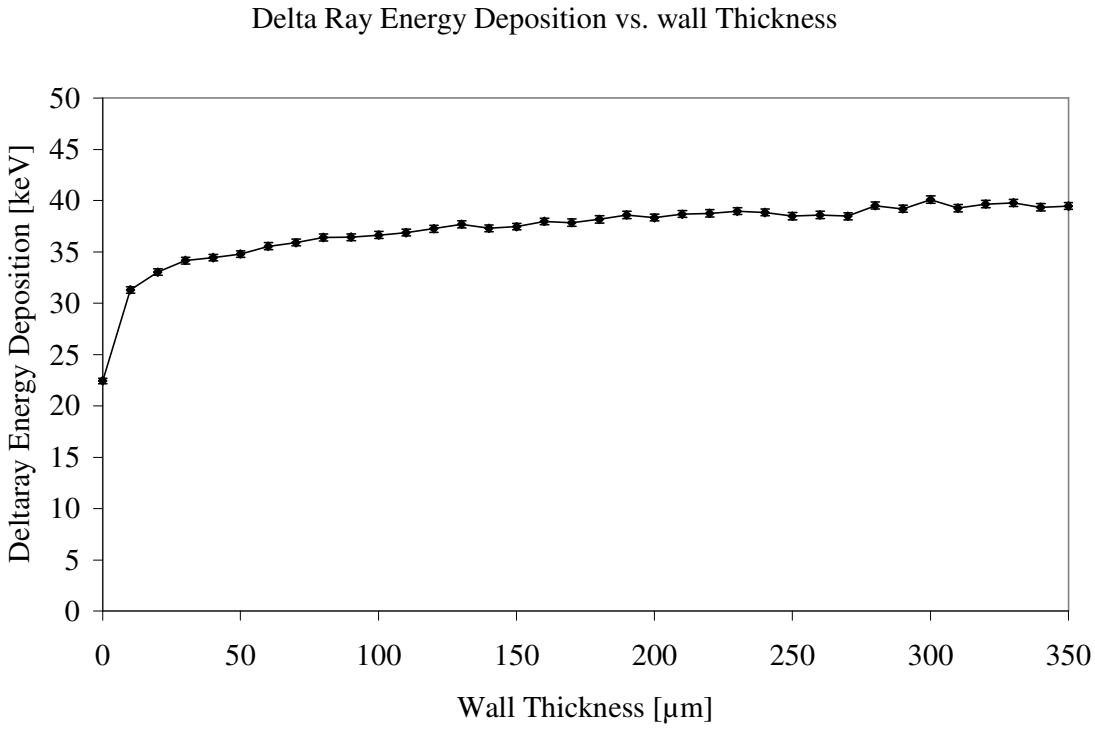

Figure 16 – Delta ray energy deposition as a function of wall thickness for a narrow ^{56}Fe beam at 360 MeV/nucleon passed down the diameter of the simulated TEPC.

To investigate the influence of wall thickness on the energy deposition in the gas, multiple narrow beams (impact parameter < 0.5 mm) were run with a varying thickness for the TE wall. This energy deposition vs. wall thickness plot is found in Fig. 16. Note, this is energy deposition from electrons (delta rays) only using the SCORE 211 FLUKA command. As expected, the energy deposition in the gas volume reaches a plateau. A recent study that modeled the response of a TEPC to neutrons using MCNPX gave similar results (Perez-Nunez 2010). From this plot alone, it could be said that a wall thickness of 300 µm would be sufficient to give the same response as the TEPC wall

(2540 µm). As the 1000 µm long TE cylinder demonstrates, however, significant delta ray energy deposition occurs past 300 µm.

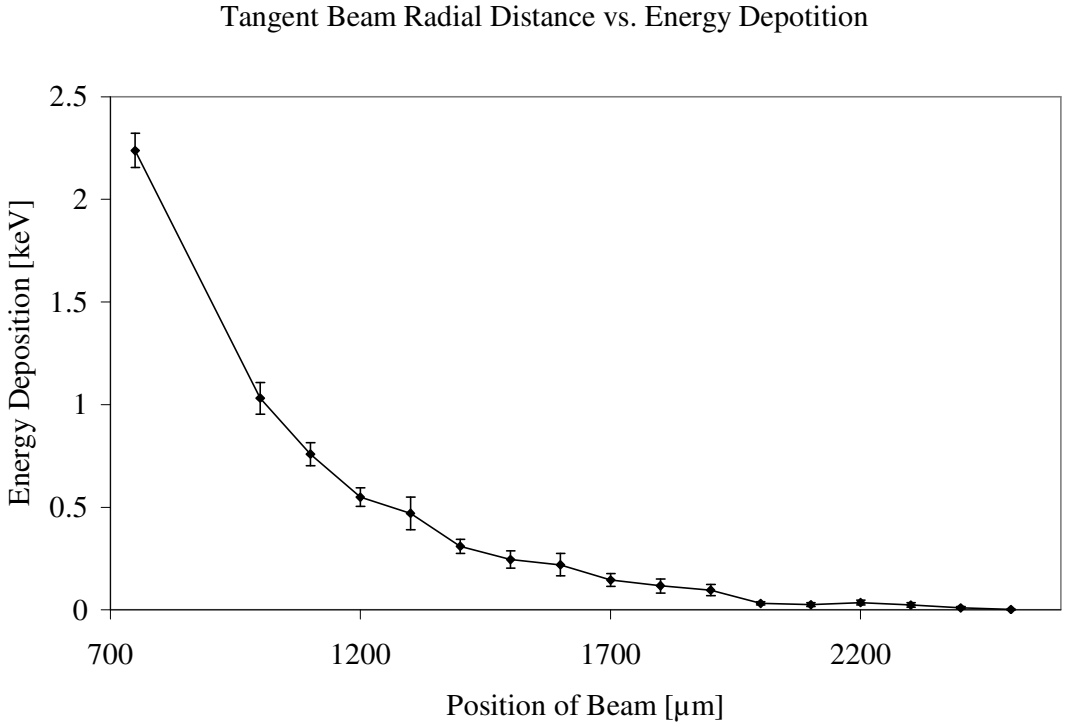

Figure 17 – Energy deposition as a function of radial distance from the gas/wall interface for a narrow ^{56}Fe beam at 360 MeV/nucleon incident on the simulated TEPC on a linear scale.

The last test in investigating how the TE wall thickness affects energy deposition in the gas involves passing a narrow beam through the simulated TEPC at various distances inside the gas/wall interface. In all cases no primary ^{56}Fe particles passed through the gas. The energy deposition vs. beam position plot appears in Fig. 17. As

expected, the energy deposition in the gas is quite small due to the delta rays travelling through hundreds or even thousands of μm of TE material.

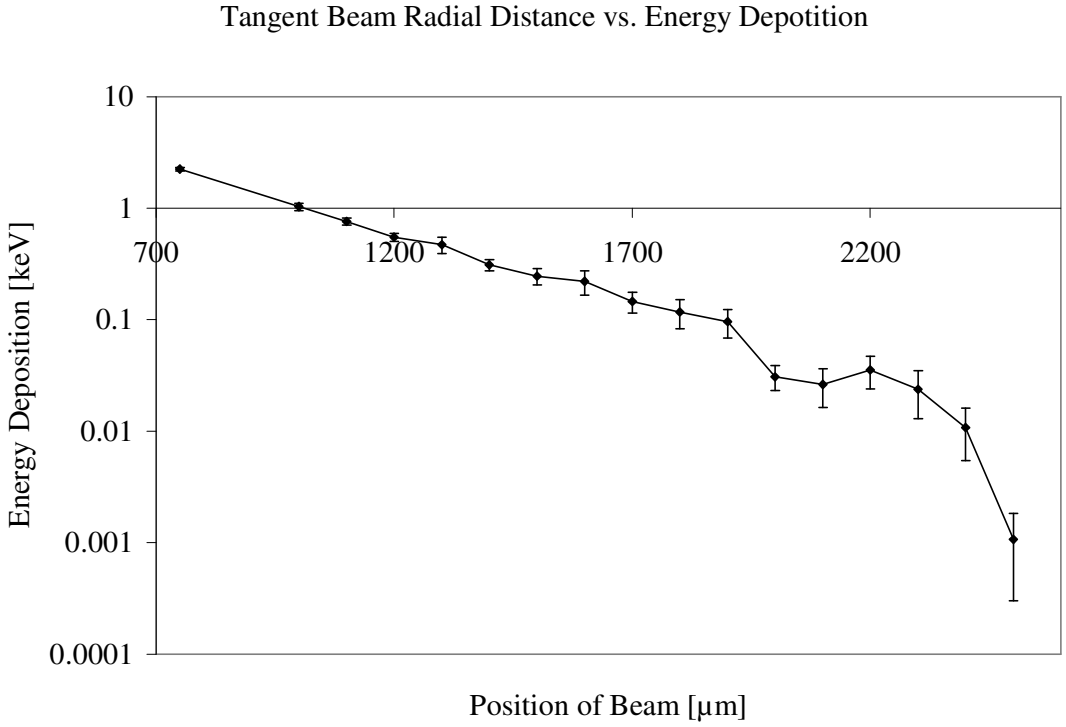

Figure 18 – Energy deposition as a function of radial distance from the gas/wall interface for a narrow ^{56}Fe beam at 360 MeV/nucleon incident on the simulated TEPC on a log scale.

The same plot appears in Fig. 18 except this time the y axis is on a log scale to bring out detail at the larger impact parameters. The 2σ error bars increases dramatically as the beam is moved further away from the gas volume. The reasoning behind this is the same as with the 1 μm TE cylinder – many of the delta rays are stopping in the TE

material. As a result, many zero energy deposition events are being included in the average which increases the standard error.

From the data gathered by the previous test (Figs. 17 and 18), a determination was made that a wall thickness of 750 µm could be used as a substitute for the original TEPC wall (2540 µm). When a narrow beam was passed 750 µm inside the TE wall, an average energy deposition of just over 2 keV was recorded. Using this 750 µm ("thin") wall vs. the original 2540 µm ("thick") wall results in a ~1% decrease in recorded energy deposition. Using a thin wall is quite beneficial for simulation purposes because of the reduced CPU time it offers.

This tradeoff was deemed acceptable for producing the plot in Fig. 19 which details energy deposition in the gas volume as a function of impact parameter from IP = 0 to IP = TE wall outer radius. Any reduction in CPU time was appreciated in producing this plot because of the many runs necessary with the beam so close to gas/TE wall interface (the longest track through the TE material therefore giving the longest runtime). This plot matches a similar plot using experimental data (Gersey 2002). The feature of interest is the spike in energy deposition close to the gas/wall interface (analyzed with the tangent beam in Fig. 7).

Plotted on the same graph is LET x chord length. As Fig. 19 shows, there is significant energy deposition in the gas volume when the beam is just inside the gas/wall interface. In that case, the chord length is 0 so LET x chord length is 0 as well. This difference is a result of delta rays depositing energy in the gas volume that were produced in the wall.

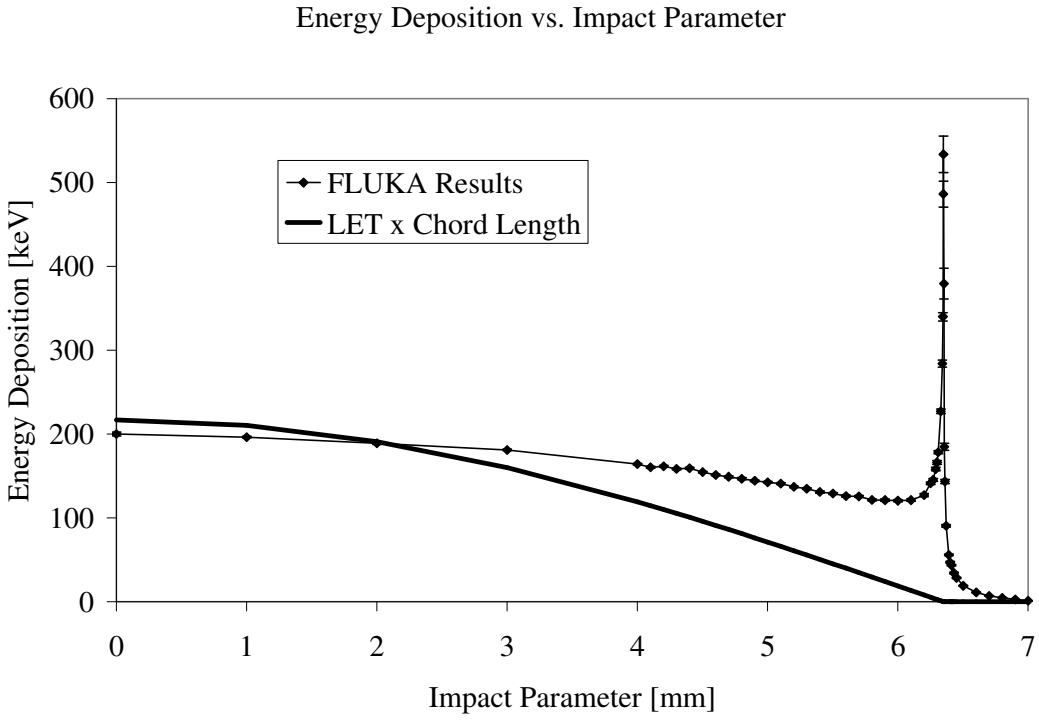

Figure 19 – Energy deposition as a function of impact parameter for a narrow ^{56}Fe beam at 360 MeV/nucleon incident on the simulated TEPC with a thin (750 µm) TE wall. In addition, LET x Chord Length is plotted to show the wall effect.

Summary of Data

To complete the analysis of the simulated TEPC, five different broad (covering surface area of detector) ^{56}Fe beams were run with energies of 200, 360, 540, 700, 790, and 1000 MeV/nucleon. These energies were chosen because of the readily available experimental data available for comparison. For all five beams, the thin wall (750 µm) was used to reduce CPU time.

Table 5 summarizes the FLUKA simulation and experimental (Gersey 2002) results.

Table 5 – Summary of y_F and y_D data

Fe-56 Beam Energy (MeV/nucleon)	Gersey y_F (keV/µm)	FLUKA y_F (keV/µm)	y_F % diff.	Gersey y_D (keV/µm)	FLUKA y_D (keV/µm)	y_D % diff.
200	199	286	43.8	328	354	7.9
360	146	196	33.9	216	246	13.7
540	134	160	19.2	173	199	15.2
700	125	144	14.9	159	181	13.9
790	118	138	17.2	153	173	13.0
1000	106	130	22.2	147	163	11.0

Table 5 contains the frequency mean lineal energy (y_F) and dose mean lineal energy (y_D) for both the Gersey experimental data and the FLUKA simulation data and their respective percent differences. From these data it can be seen that FLUKA consistently overestimates energy deposition in the simulated TEPC. The percent difference for y_F is greater than that for y_D and as a general trend, the simulation data better matched the experimental data as the beam energy increased. This is most likely due to the fact that FLUKA is primarily designed to be a high energy accelerator code and it not surprisingly benchmarked better for higher energies.

A plot of the data in Table 5 is found in Fig. 20. The FLUKA data follows the general trend of the experimental data but overestimates in all cases.

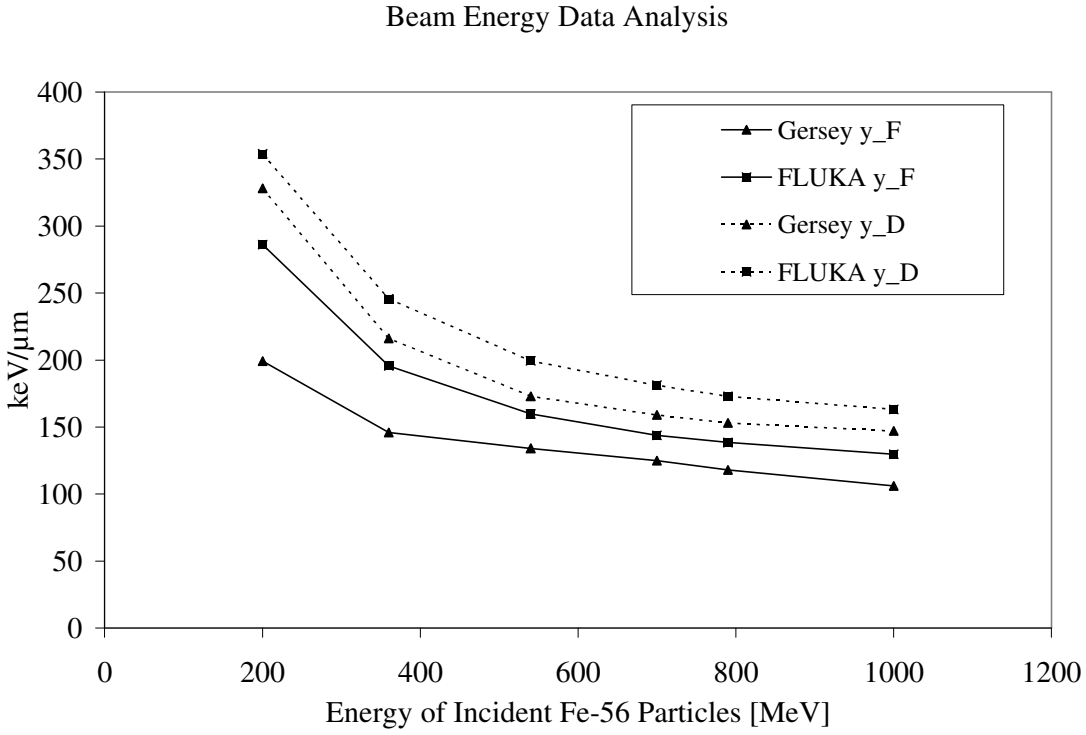

Figure 20 – Comparison of experimental (Gersey 2002) and simulation (using thin wall) frequency mean lineal energy (y_F) and dose mean lineal energy (y_D) for ^{56}Fe beams at 200, 360, 540, 700, 790, and 1000 MeV/nucleon incident on the simulated TEPC (broad beam, covering entire surface area).

CHAPTER V

CONCLUSION

A TEPC was successfully simulated using FLUKA. The main features of the broad beam spectrum were confirmed with narrow beams at different impact parameters. In addition, the TEPC was tested without FLUKA transporting delta rays (delta rays "off") and with the TE wall replaced with a vacuum.

Wall thickness was a characteristic of the detector that was studied in detail. Care was taken to ensure FLUKA responded as expected. An important end result of this wall thickness study was the determination of a suitable thinner wall to be used for the entire detector energy deposition vs. impact parameter plot and the final beam energy vs. y_F and y_D analysis. A thinner wall was desirable to reduce CPU time.

In all cases, FLUKA overestimated energy deposition in the gas volume. This is most likely due the low pressure and density of the gas. A simple test was performed where a 360 MeV/nucleon ^{56}Fe beam was passed through a 1 µm thick slab of water. For this simple test, FLUKA returned an average energy deposition equal to the expected stopping power. When the same test was run with propane, however, the energy deposition value was higher than expected (like it has been for the TEPC results).

The developers of FLUKA advertise how well it can simulate interactions at very high energies (see Table 1 – FLUKA transport limits). However, it seems the user may need to perform a slight calibration and manipulate several default values to obtain accurate results at lower energies.

Therefore, it is suggested that to ensure FLUKA gives a proper response, the MAT-PROP command (material properties) should be used. Among other things, the MAT-PROP command allows the user to override default values for ionization potential and density correction factors. With the usage of default MAT-PROP values in this study, the average percent error between the experimental and simulation data was 25.2 % for y_F and 12.4% for y_D.

REFERENCES

Attix FH. Introduction to radiological physics and radiation dosimetry. New York: Wiley & Sons; 1986.

Battistoni G, Cerutti F, Fasso A, Ferrari A, Muraro S, Ranft J, Roesler S, Sala PR. The FLUKA code: Description and benchmarking. AIP Conference Proceedings 896: 31-49; 2007.

Beck P, Ferrari A, Pelliccioni M, Rollet S, Villari R. FLUKA simulation of TEPC response to cosmic radiation. Radiation Protection Dosimetry 116 (1-4): 327-330; 2005.

Cauchy A. Memoire sur larectification des courbes et la quandrature des sourface courbe. In (ed): Oevres Completes. Paris: Gauthier Villard; 1908.

Fasso A, Ferrari A, Roesler S. FLUKA code: present applications and future developments. In the Proceedings of 2003 Conference for Computing in High-Energy and Nuclear Physics (CHEP 03). La Jolla, California: eConf C0303241:MOMT004, 2003: 1-8.

Fasso A, Ferrari A, Ranft J, Sala PR. FLUKA: a multi-particle transport code. CERN-2005-10, INFN/TC_05/11, SLAC-R-773; 2005.

Gersey BB, Borak TB, Guetersloh SB, Zeitlin C, Miller J, Heilbronn L, Murakami T, Iwata Y. The response of a spherical tissue equivalent proportional counter to 56Fe particles from 200 - 1000 MeV/nucleon. Rad. Res 157: 350-360; 2002.

Hoff J, Townsend L. MCNP modelling of the wall effects observed in tissue-equivalent proportional counters. Radiation protection dosimetry 99 (1-4): 369-70; 2002.

International Commission on Radiological Units and Measurements. Stopping power for electrons and positrons. Bethesda, MD: ICRU; ICRU Report 37; 1984.

International Commission on Radiological Units and Measurements. Fundamental quantities and units for ionizing radiation. Bethesda, MD: ICRU; ICRU Report 60; 1998.

Knoll GF. Radiation detection and measurement, 3rd ed. New York: Wiley & Sons; 2000.

National Institute of Standards and Technology. Composition of A-150 tissue-equivalent plastic [online]. Available at: http://physics.nist.gov/cgi-bin/Star/compos.pl?matno=099. Accessed 2 March 2010.

Perez-Nunez D, Braby L. Effect of wall thickness on measurement of dose for high energy neutrons. Health Physics 98 (1): 37-41; 2010.

Rollet S, Beck P, Ferrari A, Pelliccioni M, Autischer M. Dosimetric considerations on TEPC FLUKA-simulation and measurements. Radiation Protection Dosimetry 110 (1-4): 833-834; 2004.

Rossi HH, Zaider M. Microdosimetry and its applications. New York: Springer; 1996.

Vavilov, PV., Ionization losses of high-energy heavy particles. Soviet Physics - JETP 5 (4): 749-751; 1957.

Wang, X. Monte Carlo simulations of solid walled proportional counter with different site size for HZE radiation. Thesis (M.S.): Texas A&M University; 2006.

VITA

Name: Jeremy Dell Northum

Address: Texas A&M University
Department of Nuclear Engineering
3133 TAMU
College Station, TX 77843-3133

Email Address: jnorthum@neo.tamu.edu

Education: B.S., Nuclear Engineering, Texas A&M University, 2008
M.S., Health Physics, Texas A&M University, 2010